NEW NON-SUPERCONDUCTING MODULATION-FREE BiPbSr$_2$MO$_y$ PHASES (M=Co, Mn, Fe) ISOTYPIC WITH THE 10 K Bi$_2$Sr$_2$CuO$_y$ SUPERCONDUCTOR

J.M. TARASCON, Y. LePAGE [a], W.R. McKINNON [a], R. RAMESH, M. EIBSCHUTZ,
E. TSELEPIS [a], E. WANG and G.W. HULL

Bell Communications Research, Red Bank, NJ 07701, USA

[a] *National Research Council of Canada, Ottawa, K1A OR9, Canada*

[b] *AT&T Bell Laboratories, Murray Hill, NJ 07974, USA*

Bi can be replaced by Pb in the phases Bi$_2$Sr$_2$MO$_y$ (M=Co, Mn, Fe), which are isostructural to the 10 K superconductor Bi$_2$Sr$_2$CuO$_y$ but have a transition metal M substituted for Cu. New non-superconducting phases with the formula BiPbA$_2$MO$_6$ (A=Sr, Ca; M=Fe, Co and Mn) were prepared in a reducing atmosphere. Single crystals of these phases were grown using excess PbO–Bi$_2$O$_3$ as a flux, and their structural, magnetic and electrical properties were studied. The structure of BiPbSr$_2$MnO$_6$ was solved by single crystal X-ray diffraction studies, and show no modulation, in contrast to Bi$_2$Sr$_2$MO$_y$, where the structure is strongly modulated by a bending of the perovskite slabs. In the (Pb, Bi)O layers, the (Pb, Bi) and O atoms form ribbons along the a-axis. There are only six oxygens per formula, so the Mn is in the 3+ oxidation state. Mössbauer measurements for M=Fe confirm this oxidation state. The lack of an extra oxygen in the (Pb, Bi)O layers is consistent with the lack of the modulation, since extra oxygen accompanies the structural modulation in Bi$_2$Sr$_2$MO$_y$. The modulation can be introduced reversibly in Bi-PbSr$_2$MnO$_6$ by heating it under oxygen near 500°C, directly showing for the first time the correlation between oxygen and the modulation. All the Pb substituted phases are insulating, and some show magnetic phase transitions. Although the magnetic transition temperatures are comparable to those in Bi$_2$Sr$_2$MO$_y$, the peaks in magnetic susceptibility are weaker, probably because there is no modulation.

1. Introduction

Since the first report of superconductivity by Bednorz and Muller [1] in the La–Ba–Cu–O system, each new high-T_c cuprate system discovered has shown both peculiar structural aspects (such as the CuO chains in the YBa$_2$Cu$_3$O$_7$ materials [2–4] (denoted 123) or a modulation of the structure for the Bi-based cuprate [5–7]) and simultaneously higher superconducting transition temperatures (for instance 90 K for the 123 phase or 110 K and 125 K for the Bi or Tl based materials [8,9], respectively). With each discovery, chemists and theoreticians have tried to correlate these structural anomalies to the higher values of T_c. This correlation was rapidly dismissed by means of chemical substitutions in the 123 system [10–11]. We recently replaced Cu by 3d metals in the high-T_c Bi-cuprates of general formula Bi$_2$Sr$_2$Ca$_{n-1}$Cu$_n$O$_y$ ($n=1, 2, 3$) and discovered new insulating compounds isostructural with the cu-

prates (but with a commensurate modulation) [12–14]. Single crystal X-ray studies [15,16] on these phases revealed the mechanism for the structural modulation (the periodic insertion of a row of oxygen atoms within the Bi–O layers), but failed to answer why the periodicity of this modulation locks to an integer number such as 4 for the $n=1$ phase or 5 for the $n=2$ phase. In addition to their interesting structural properties [12,14], most of the 3d-metal substituted phases have also shown novel magnetic properties, with strong peaks in the susceptibility that are probably due to the structural modulation.

It has been previously shown by High Resolution Electron Microscopy (HREM) [17] that the substitution of 0.35 Bi by 0.35 Pb in the Bi$_2$Sr$_2$Ca$_2$Cu$_3$O$_y$ phase doubles the periodicity of the modulation from 4.6 to 9.2 times the subcell repeat distance. It is also reported that the replacement of one Bi by Pb in Bi$_2$Sr$_2$YCu$_2$O$_y$ destroys the modulation [18]. Thus we decided to investigate the substitution for Bi by

Pb in the new 3d metal substituted phases and succeeded in preparing (in bulk or single crystal form) a new family of single phase materials of formula $Bi_{2-x}Pb_xSr_2MO_y$, (M=Mn, Co and Fe) centered around $x=1$. These materials are isostructural to the 10 K Bi-based cuprates but lack the structural modulation. Here we report the synthesis, crystal structure and physical properties of these new phases and compare our results to the properties of the modulated structures.

2. Synthesis

The compounds $Bi_{2-x}Pb_xSr_2MO_y$, ($x=0$ to 1.5; M=Co, Mn and Fe) were prepared from Bi_2O_3, PbO, 3d metal oxides (MnO_2, Co_3O_4 or Fe_2O_3), each of purity greater than 99% and carbonates for the divalent alkaline earths (Sr, Ca). Amounts appropriate to form 2 g samples were thoroughly mixed, separated in 2×1 g samples and then placed into alumina crucibles. For each preparation, one set of samples was treated in air and another in nitrogen. Solid state reactions carried out in air produce multiphase samples, independently of Pb content (x) or annealing temperatures and times. In contrast, when the mixed powders are heated in a nitrogen ambient, single phase $Bi_{2-x}Pb_xSr_2MO_y$ materials (with no trace of impurity phases) are formed for values of x close to 1. The synthesis conditions of these new phases, either in bulk or single crystal form, depend strongly on the 3d metal (M).

For the Mn series, an annealing treatment at temperatures of 960°C for 2 days under nitrogen is required to produce single phase materials. Among the series of samples investigated, only those for x ranging from $0<x<0.6$ and from 0.8 to 1.2 were single phase (as determined by powder X-ray diffraction). In this study the lower or upper limit of range of solubility are taken as the value of x for which the last compound is still single phase; because it is difficult to detect phases below a level of 5% by powder X-ray diffraction, the solubility limits quoted here are accurate to about 0.1. Figure 1 shows the variation of a and b as a function of x. All the Bragg peaks can be fitted to an orthorhombic cell denoted O(1) (with $a=4×5.43$ and $b=5.42$) at low $x(0<x<0.6)$, and to a second orthorhombic cell denoted O(2) for

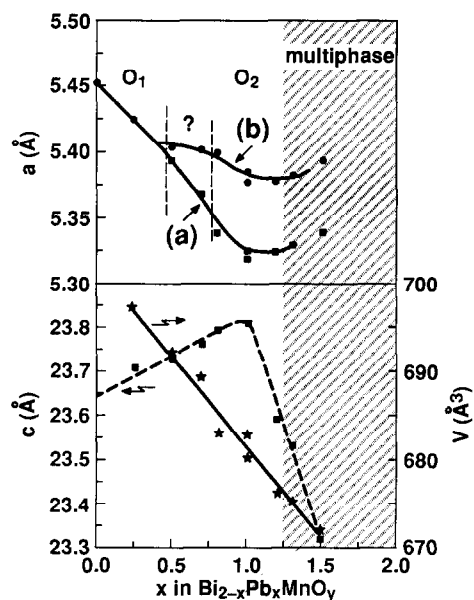Fig. 1. Unit cell parameters (a, b, c and V) as a function of the Pb content (x) in $Bi_{2-x}Pb_xMnO_y$. The solid and dashed lines joining the experimental points are guides to the eyes.

$0.8<x<1.2$. Between these two ranges of composition, the O(1) and O(2) phases seem to coexist suggesting a non-continuous structural phase transition. Non-stoichiometry is probably responsible for the large change in the c-axis for x larger than 1, but we have not confirmed this. Similar phases with Ca instead of Sr ($BiPbCa_2MnO_y$) can also be made in N_2. The lattice parameters are given in table I.

Using similar conditions but with annealing temperatures 30°C higher, we obtained single phase $Bi_{2-x}Pb_xSr_2FeO_y$, with x ranging from 0.9–1.2. Outside this range the phases do not form. In the 2201 Bi phase [12], the substitution for Cu by Fe is limited to 50% ($Bi_2Sr_2Cu_{0.5}Fe_{0.5}O_y$), but with 50% of the Bi replaced by Pb, the 2201 phase with only Fe can be made. Like the Mn system, the Fe 2201 phase also forms with Ca (lattice parameters shown in table I), but is difficult to synthesize free of impurity phases.

The Co equivalent of the Fe 2201 or Mn 2201 Bi phases were prepared at 860°C in N_2. This annealing temperature is about 100°C lower than for the Fe or Mn phases. As for Mn, a single phase material forms near $x=1$ with a similar range of solubility

Table I

Crystallographic lattice parameters for the new phases BiPb(SrCa)$_2$MO$_6$ and the parent phases Bi$_2$(SrCa)$_2$MO$_6$ phases. The periodicity of the structural modulation (p) is indicated by bold numbers. The Pb-doped samples do not show a structural distortion, as determined by both single crystal X-ray and HREM studies. Where possible, the lattice parameters for single crystals are given.

Compounds	$p \times a$ (Å)	b (Å)	c (Å)	V (Å^3)
Bi$_2$Sr$_2$MnO$_{6.25}$	**4**×5.451(2)	5.426(2)	23.613(8)	698.40
BiPbSr$_2$MnO$_6$	5.331(0)	5.399(1)	23.751(2)	683.77
Bi$_2$Ca$_2$MnO$_{6.25}$	**4**×5.343(2)	5.360(1)	23.151(2)	663.0
BiPbCa$_2$MnO$_6$	5.218(0)	5.346(2)	23.467(10)	654.65
Bi$_2$Sr$_2$CoO$_{6.25}$	**4**×5.459(5)	5.426(2)	23.450(4)	699.15
BiPbSr$_2$CoO$_6$	5.326(1)	5.396(1)	23.521(3)	675.97
BiPbSr$_2$FeO$_6$	5.416(1)	5.505(1)	23.215(4)	693.69
BiPbCa$_2$FeO$_6$	5.347(1)	5.502(1)	23.766(2)	669.80

($0.8 < x < 1.1$). For the single phase samples, all the Bragg peaks were indexed on an orthorhombic unit cell and the lattice parameters are reported in table I. Again, as for the Mn or Fe phases for x close to 1, the X-ray powder patterns do not contain weak reflections associated with the modulation in the Pb-free samples, suggesting that the structural distortion has disappeared, as was confirmed (see below) by single crystal and High Resolution Electron Microscopy studies.

Crystals of the BiPbSr$_2$MO$_y$ (M = Co, Fe, and Mn) phases were grown in an alumina crucible under N$_2$ with a 22 g load of composition Bi:Pb:Sr:M = 1.5:1.5:2:1. The 50% excess of Bi$_2$O$_3$ and PbO serves as the flux. The samples were heated to a temperature T_1 in 8 h, held at T_1 for 1.75 h, then cooled to 800°C in 50 h. The growth temperature T_1 depends on the nature of M: 1300°C for BiPbSr$_2$MnO$_6$ crystals, 1200°C for BiPbCa$_2$MnO$_6$ crystals and 1080°C for crystals of the Fe and Co phases. The fast heating partially melts the materials and generates large cavities containing free thin crystals ranging from several micrometers to 5 or 6 mm. These crystals were used for the structural and physical measurements reported here.

For the Fe system, attempts to grow the $n = 1$ phase at higher temperatures (1250°C) produced the $n = 2$, BiPbSr$_3$Fe$_2$O$_y$, phase. This phase has $c = 31.89$ Å, compared to 31.69 Å for Bi$_2$Sr$_3$Fe$_2$O$_y$. This increase in c is similar to the increase from 23.60 Å to 23.71 Å when one Pb atom replaces one Bi atom in the $n = 1$ phase.

In order to determine the oxygen content for these materials we performed thermogravimetric analysis measurements (TGA). In such measurements the weight loss of a sample placed in a Pt boat under a reducing ambient (Ar/H$_2$ mixture) is monitored as a function of the heating temperature while the samples are heated up to 900°C at 10°C/min. From the weight loss of the samples we consistently obtained an oxygen content y in BiPbSr$_2$MO$_y$ of 6.05 and 6.1 ± 0.05 for M = Fe and Co, respectively. Such an oxygen content implies that, in order to maintain charge neutrality, Pb is in its 2+ oxidation state and the 3d metal (M) is in its 3+ oxidation state. For comparison, in the undoped phase Bi$_2$Sr$_2$CoO$_y$, a value of $y = 6.54$ was obtained in the TGA analysis, indicating that the replacement of one Bi by one Pb atom in Bi$_2$Sr$_2$CoO$_y$ is accompanied by the loss of 0.5 oxygen atom. For the Mn based materials, because of a reaction with the Pt container, TGA measurements failed in determining oxygen content.

3. Structure of BiPbSr$_2$MnO$_6$

A 0.2×0.1×0.02 mm^3 BiPbSr$_2$MnO$_6$ platelet crystal was selected from a batch prepared at 1300°C as described above. X-ray diffraction of MoKα radiation showed the cell to be A-face centered orthorhombic with edges $a = 5.3311(4)$, $b = 5.3988(6)$, $c = 23.7574(73)$ Å, with no indication of modulation in the (001) plane, in agreement with electron-diffraction studies. All reflections with h, k and l of different parity were weak, indicating a prominent pseudo F-centered cell. (In fact, these lines are not visible in our measured powder patterns). Intensity measurements were performed up to 60 degrees Bragg

angle with graphite-monochromatized MoKα radiation on a CAD-4 diffractometer controlled by NRCAD control programs [19]. After correction for absorption, the 3844 measurements merged to 618 unique reflections with $R_{merge}=7.3\%$, a high value due to the large range of the absorption correction. Analysis of those reflections indicated two probable space groups. Amaa (#66) and A2aa (#37). Only three of the 61 unique measurements of systematic absences were larger than 2.5 counting statistics sigma, while 427 of the 557 valid unique measurements were observed at that level. Structure solution by direct methods in space group Amaa showed the well known substructure of the 2201 phase [22], with ribbons of strong Bi-O bonds, and splitting of the oxygen site in the Bi plane. This disorder clearly corresponded to two orientations of three mutually perpendicular bonds, a common stereochemistry for Bi^{3+}. Lowering the symmetry to A2aa and full-matrix refinement of this model gave an ordered structure with the same residual ($R_F=6.2\%$). The space group A2aa gives ribbons of BiO, as discussed below. Because each Bi has two equidistant Bi neighbors in the BiO layer, we ruled out space groups that resolve the disorder in Amaa through the formation of diamonds of Bi_2O_2, because this would produce one short Bi-Bi distance, not two equal ones. Anomalous scattering was taken into account, but the parameter η was kept at 0.5 (equal amounts of both polarities) and not refined.

The essential details of the structure are given in table II; II(a) gives the atomic positions and isotropic thermal parameters, II(b) the anisotropic thermal parameters, and II(c) the important interatomic distances. (The observed and calculated structure factors are available from the authors on request.) Observed and calculated powder patterns are compared in table III. All calculations were performed by use of the NRCVAX system of programs [19-20].

As can be seen from these tables, the stereochemistry of the various ions is as expected for this structure type. Mn is in 4+2 coordination with 4 coplanar and equal bond lengths of 1.90(7) Å and two perpendicular bond lengths of 2.33(3) Å, leading to a bond-valence sum of 3.2 valence units (using the bond-valence parameters of Brown and Altermatt [21] for Mn^{3+}). Sr is in its familiar 9-coordinated

site, with large angular distortion of the apical oxygen but similar bond lengths (in the range 2.58(5)-2.72(5) Å, with a bond-valence sum of 2.01). Bi and Pb occupy randomly a distorted octahedron with 3 mutually perpendicular bonds (90±2°) which are short and equal in length (2.20±4 Å) and three longer bonds around 3.1 Å, leading to a bond-valence sum of 2.35 for Bi and 2.46 for Pb, roughly midway between the expected value of Bi^{3+} and Pb^{2+}. Because Bi and Pb have virtually identical scattering amplitudes for X-rays, we could not expect to see ordering of the Pb and Bi directly, but we see no evidence of such ordering in the bonds to oxygen.

The metal and oxygen positions projected onto the *a-c* plane are shown in fig. 2(a) and (b) for $Bi_2Sr_2MnOᵧ$ and $BiPbSr_2MnO_6$, respectively. In this projection, the modulation of $Bi_2Sr_2MnOᵧ$ appears as a bending of the perovskite slabs. Replacing Bi by Pb to form $BiPbSr_2MnO_6$ removes the modulation, so the slabs are flat. Because of the distortion, the octahedra of MnO_6 tilt left or right in $Bi_2Sr_2MnOᵧ$. The octahedra in $BiPbSr_2MnO_6$ do not tilt in this projection, but they are tilted in the *b-c* plane, reminiscent of the tilting in La_2CuO_4, as shown by the projection in fig. 3(a). The oxygen above and below the Mn, in the SrO layer, are noticeably shifted left or right of the Sr in the same layer, corresponding to a rotation of the MnO_6 octahedra about an axis along *a*. (This rotation also probably shifts the other oxygen in the MnO_6 octahedra slightly out of the *a-b* plane of the Mn atoms, but although such a shift can be seen in fig. 3(a), it is smaller than the uncertainty in the *z*-coordinate of the oxygen position.) The chains in the (Bi, Pb)O layers of $BiPbSr_2MnO_6$ can be noted in both fig. 2(a) and fig. 3(b). In the *a-c* plane (fig. 2(a)) the oxygen atoms are always to the left of the (Bi, Pb) atoms; in the *b-c* plane (fig. 3(a)) pairs of oxygen atoms are between pairs of (Bi, Pb) atoms. (In the *a-c* projection of $Bi_2Sr_2MnOᵧ$, O atoms may lie either left or right of Bi, because the chains do not extend throughout the layers). The reason for these positions is evident in the view of the chains in fig. 3(b), a projection in the *a-b* plane of (Bi, Pb) and O positions, showing the chains running along the *a-* axis.

This is the first observation of oxygen ordering in the subcell of a Bi-containing analog of the 2201 su-

Table II

Crystal data for $BiPbSr_2MnO_6$. The numbers in parentheses are the estimated standard deviation of the last digit printed. (a) The atomic parameters x, y, z and the mean of the principle axes of the thermal ellipsoid, B_{iso}. The unit of B_{iso} is $Å^2$.

	x	y	z	B ($Å^2$)
Bi	0.00000	0.23748(23)	0.06151(6)	1.09(12)
Sr	0.0034(21)	0.7507(5)	0.17245(14)	0.95(21)
Mn	−0.001(6)	1/4	1/4	1.00(23)
O 1	0.255(14)	0.008(13)	0.2483(9)	1.1(3)
O 2	0.002(17)	0.274(5)	0.1522(10)	1.5(4)
O 3	0.410(7)	0.152(6)	0.0662(13)	1.7(5)

(b) The anisotropic temperature parameters $u(i,j)$ in units of $Å^2(\times 10^2)$.

	u_{11}	u_{22}	u_{33}	u_{12}	u_{13}	u_{23}
Bi	1.55(7)	1.13(6)	1.47	0.3(3)	0.40(18)	−0.01(4)
Sr	1.12(15)	0.88(12)	1.62(14)	0.4(3)	−0.6(5)	−0.16(10)
Mn	0.7(3)	0.8(3)	2.4(3)	0.000	0.000	0.04(25)

Anisotropic Temperature Factors are of the form: $T = -2\pi^2(h^*h^*u_{11}a^+... +2hku_{12}a^*b^*+...)$.

(c) The important interatomic distances in Å.

Bi–O(2)	2.16(3)	Sr–O(1)	2.64(5)
Bi–O(3)	2.23(4)	Sr–O(1)	2.71(5)
Bi–O(3)	3.18(4)	Sr–O(1)	2.58(5)
Bi–O(3)	3.33(3)	Sr–O(1)	2.64(5)
Bi–O(3)	2.16(3)	Sr–O(2)	2.86(3)
Bi–O(3)	3.11(3)	Sr–O(2)	2.62(5)
		Sr–O(2)	2.70(9)
Mn–O(1)	1.89(7)×2	Sr–O(2)	2.72(9)
Mn–O(1)	1.91(7)×2	Sr–O(3)	2.63(3)
Mn–O(2)	2.33(3)×2		

perconductor. The ribbons or strong bonds postulated by Subramanian et al. [7,22] and seen over distances of about 20 Å in $Bi_2Sr_3Fe_2O_{9.2}$ by LePage et al. [15] are here visible and ordered, probably over domains. The 0.073(1) Å displacement of Bi atoms to form ribbons is small, but highly significant. It is in fact responsible for the major part of the intensity violations of the pseudo F-centering.

The formation of these chains may result from the pronounced covalent character of Bi. Chains are observed, for example, in Bi_2MoO_6, but the additional oxygens in Aurivilius positions between the BiO layers [23] also bond strongly to the Bi. Within the ribbons the Bi–O–Bi angle is of 115°C, in contrast to 90° or 180° for a pure rocksalt or a pure perovskite layer, respectively. This angle is probably related to the covalency of the Bi–O–Bi bonds through the hybridization of Bi 6s and O 2p, and being able to vary,

it should lead to elasticity of the BiO layer. Because of this elasticity, one might expect compounds with a wide range of difference between the a and b lattice parameters. This is not so (the difference in a and b for the compounds reported in table I does not exceed 2.8%), presumably because of constraints imposed by the other layers in the structure.

The new Pb doped 2201 phases ($BiPbSr_2MnO_6$) were further studied by high resolution electron microscopy (HREM) using a 0.27 micron area aperture. The electron diffraction patterns corresponding to the zones [010] [100], and [001] for the BiPbSr₂MnO₆ compound are displayed in fig. 4(b), (c) and (d), respectively, together with for comparison an electron diffraction pattern corresponding to the [010] zone for the $Bi_2Sr_2MnO_y$ compound taken using experimental conditions similar as in fig. 4(b), (c) and (d). In fig. 4(a) there are seven rows

Table III
Observed and calculated powder pattern for $BiPbSr_2MnO_6$. The values of 2 T are for Cu radiation.

D-space	Int$_{cal}$	h	k	l	2θ	Int$_{obs}$	D-space	Int$_{cal}$	h	k	l	2θ	Int$_{obs}$
11.88	20	0	0	2	7.44	8	1.5906	15	3	1	5	57.93	13
5.265	2	0	1	1	16.83		1.5894	1	2	0	12	57.98	2
3.960	7	0	0	6	22.44	13	1.4848	2	0	0	16	62.50	4
3.746	3	1	1	1	23.73	3	1.4822	7	2	2	10	62.62	6
3.421	55	1	1	3	26.02	55	1.3696	1	2	2	12	68.45	
2.9697	21	0	0	8	30.07	19	1.3497	3	0	4	0	69.60	
2.9645	100	1	1	5	30.12	100	1.3383	3	1	3	11	70.28	2
2.6994	31	0	2	0	33.16	27	1.3328	3	4	0	0	70.62	4
2.6655	30	2	0	0	33.59	27	1.3300	3	3	1	11	70.79	4
2.6323	3	0	2	2	34.03	3	1.3199	1	0	0	18	71.41	
2.6009	3	2	0	2	34.46	3	1.3113	1	1	1	17	71.95	
2.5293	1	1	1	7	35.46		1.3010	2	0	2	16	72.61	7
2.3757	11	0	0	10	37.84	17	1.2972	2	2	0	16	72.86	7
2.2304	1	0	2	6	40.41		1.2486	2	3	3	3	76.18	
2.2112	1	2	0	6	40.77		1.2467	5	1	3	13	76.32	3
1.9975	15	0	2	8	45.37	19	1.2400	5	3	1	13	76.81	2
1.9837	15	2	0	8	45.70	15	1.2287	2	0	4	8	77.64	2
1.9798	2	0	0	12	45.79		1.2219	6	3	3	5	78.16	3
1.8967	24	2	2	0	47.92	20	1.2159	2	4	0	8	78.62	2
1.8769	9	1	1	11	48.46	10	1.2041	3	2	4	0	79.54	2
1.8730	1	2	2	2	48.57		1.1951	3	4	2	0	80.27	2
1.7834	0	0	2	10	51.18		1.1857	2	0	2	18	81.03	2
1.7735	6	2	0	10	51.48	6	1.1828	2	2	0	18	81.27	
1.7106	2	2	2	6	53.53		1.1735	1	0	4	10	82.05	
1.6669	7	1	3	3	55.05	6	1.1692	3	2	2	16	82.42	4
1.6509	7	3	1	3	55.63	6	1.1624	1	4	0	10	83.01	
1.6464	14	1	1	13	55.79	19	1.1159	3	2	4	8	87.31	2
1.6049	16	1	3	5	57.37	13	1.1086	3	4	2	8	88.02	2
1.5985	11	2	2	8	57.62	11	1.0912	1	3	3	11	89.81	
1.5964	1	0	2	12	57.70								

of weak spots equally spaced between the 000 and 200 subcell reflections, indicating a commensurate modulation of multiplicity 4. These rows of weak spots are absent in fig. 4(b) indicating, in agreement with our X-ray work, the disappearance of the structural modulation with the substitution of one Bi atom by one Pb in $Bi_2Sr_2MnO_y$. Figure 4(b) shows reflections of the type 0kl with k+l even, in agreement with the A-face centering type. The reflections with k and l odd are all weak, in agreement with the pronounced pseudo F lattice type. Figure 4(c) shows that among the h0l reflections, the h odd reflections are absent according to the a glide plane perpendicular to b. Figure 4(d) shows the hk0 reflections. The reflections with h and k even are strong, in agreement with the pseudo F centering. The reflections with k odd are absent, in agreement with the A-face

centering, and those with h odd, forbidden by the a glide plane, are also absent. Although not visible in figure 4(d), very weak reflections are present that correspond to a superlattice in which b is doubled. (These reflections become more noticeable after the oxygen treatment to be described below; see fig. 7.) These reflections, which could not be seen with X-rays, may correspond to some partial ordering of Bi and Pb along the b-direction.

The disappearance of the structural modulation with increasing x in $Bi_{2-x}Pb_xSr_2MnO_y$ was studied by electron diffraction for five samples, with x ranging from 0 to 1 in 0.25 steps. For x=0, the modulation is commensurate along a, with a q vector of 0.25a*, corresponding to a wavelength 1/q of four times the subcell lattice parameter. For x=0.25, the modulation becomes slightly incommensurate, and
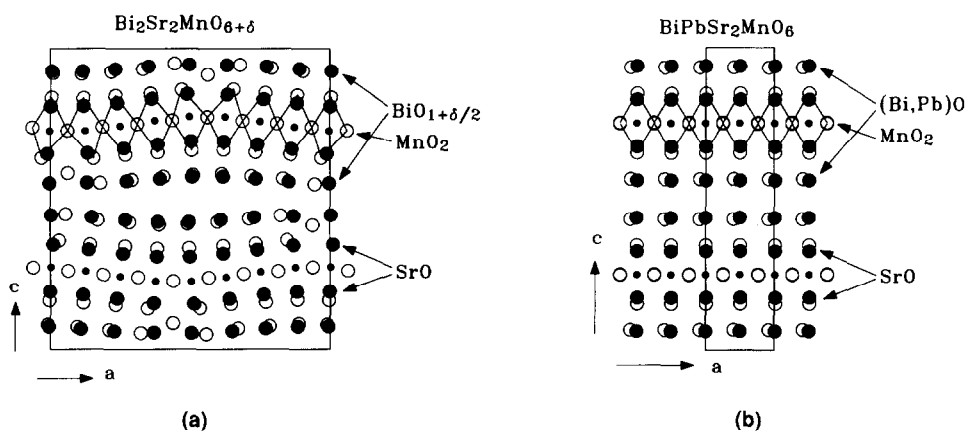
Fig. 2. (a) Projection of the structure of $Bi_2Sr_2MnO_{6+y}$ in the a-c plane, showing the modulation of the structure. The large solid circles are Bi or Sr, the small solid circles are Mn, and the open circles are O. Solid lines outline the unit cell and join the oxygen that make up the MnO_6 octahedra. The atomic coordinates are from Tarascon et al. [26]. (b) Projection of the structure of $BiPbSr_2MnO_6$ in the a-c plane, showing the absence of the modulation. In this projection, each (Bi, Pb) appears just to the right of an O in the (Bi, Pb)O layers, a sign of the (Bi, Pb)O chains. The solid lines outline the MnO_6 octahedra and the unit cell. There is no tilting of these octahedra in this projection.
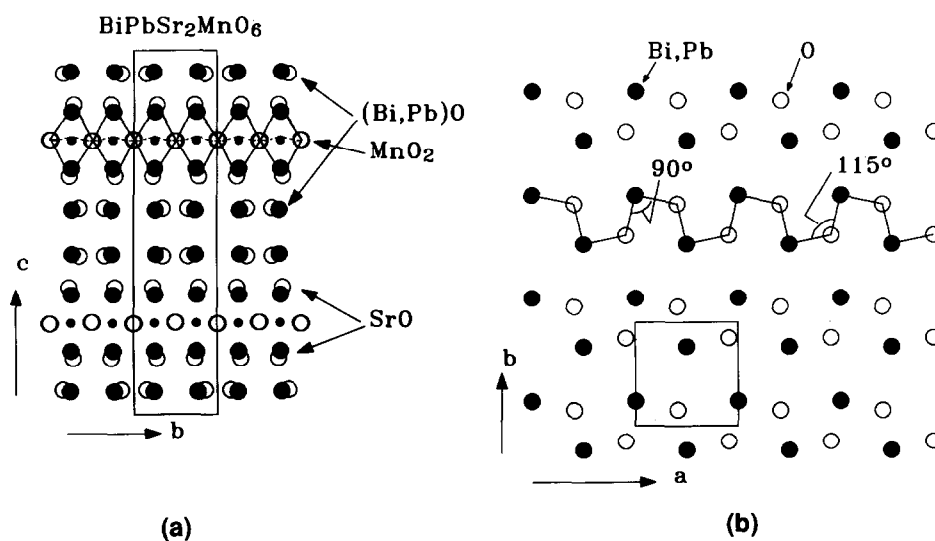
Fig. 3. (a) Projection of the structure of $BiPbSr_2MnO_6$ in the b-c plane. In this projection, the chains of (Bi, Pb)O are viewed end on, and pairs of O atoms lie between pairs of (Bi, Pb) atoms. The solid lines in the upper part of the figure outline the MnO_6 octahedra. Because the oxygen in the SrO layers are shifted either left or right of the Sr atoms (because of their strong bonds to the (Bi, Pb) in the adjacent layer), these octahedra tilt alternately left or right along the b-direction. (b) A layer of (Bi, Pb)O from $BiPbSr_2MnO_6$. The atoms in one set of chains of (Bi, Pb)O are joined, and the angles O–Bi–O and Bi–O–Bi are indicated.

the wavelength of the modulation increases from 4 to 4.16(2). Otherwise, the modulation is similar to that at $x=0$. For $x=0.50$, the modulation is incommensurate, and $1/q$ has increased to 6.9(2) along a.

The diffraction pattern now has little resemblance with that for $x=0$. The pattern at $x=0.75$ is similar to that for $x=0.5$, with a further increase in $1/q$ to 7.5(2). Moreover, at $x=0.75$ there is a second, com-
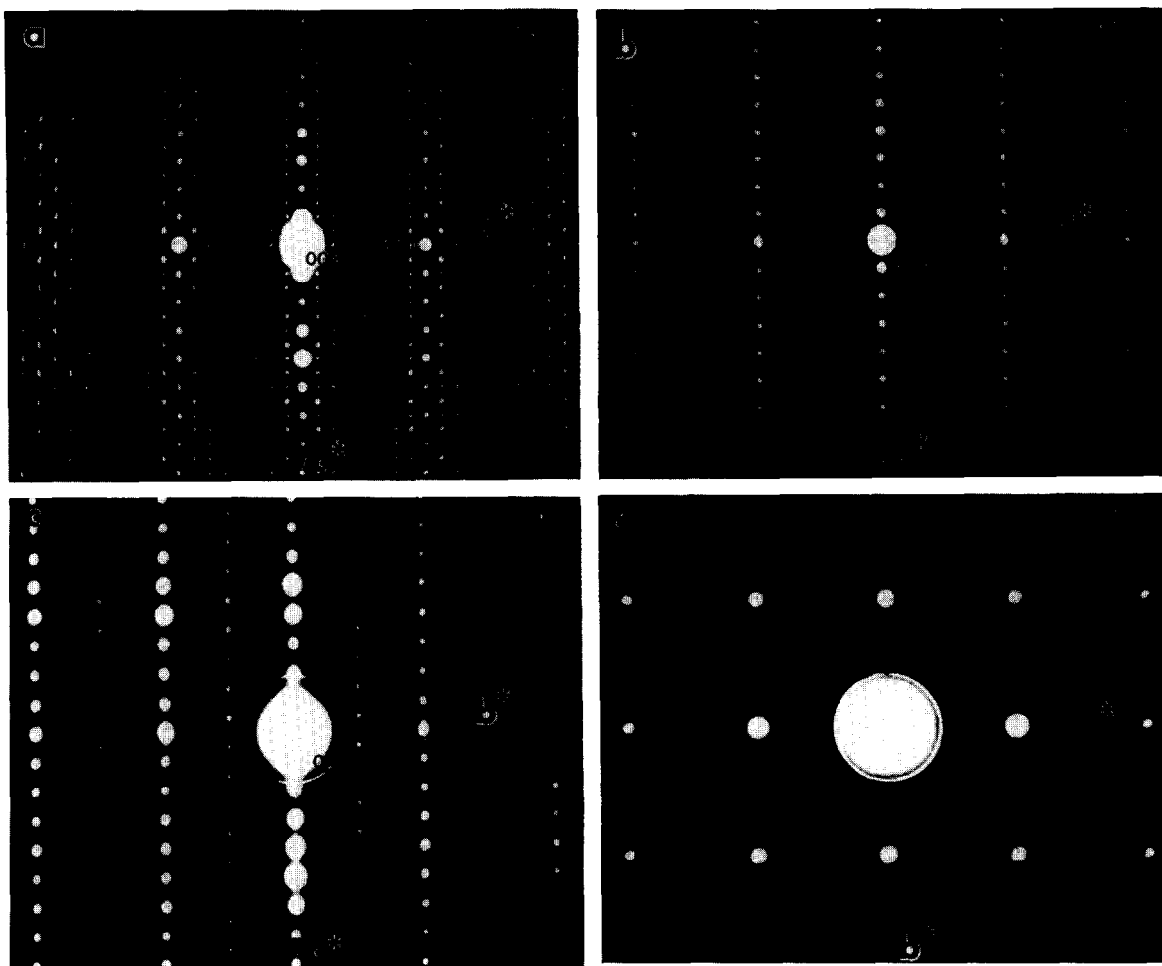
Fig. 4. Selected-area electron diffraction patterns along the 010 direction for (a) $Bi_2Sr_2MnO_y$ and (b) $BiPbSr_2MnO_6$. The electron diffraction patterns for $BiPbSr_2MnO_6$ taken along the 100 and 001 direction are shown in (c) and (d), respectively.

mensurate modulation, in the *b*-direction. This pattern with both modulations is seen in different parts of the sample, and so is probably due to two simultaneous modulations, not to two phases with different modulations. At $x=1$, all the spots associated with the modulation disappear, except for those mentioned above that might be related to an ordering of Pb and Bi.

The ^{57}Fe Mössbauer effect has been used to further study the local structure and the valence of Fe in $BiPbSr_2FeO_y$. Figure 5 shows the ^{57}Fe Mössbauer absorption spectra for $BiPbSr_2FeO_y$ in standard transmission geometry with a ^{57}Co in Rh source, and

compares it to the spectrum obtained previously [12] in similar conditions for the modulated compound $Bi_2Sr_2Cu_{0.6}Fe_{0.4}O_y$. The two spectra are significantly different. The Mössbauer spectrum of $BiPbSr_2FeO_y$ material shows two resonance lines due to a nonzero electrical field gradient at the iron nucleus (fig. 5(b)). In contrast, for $Bi_2Sr_2Cu_{1-x}Fe_xO_y$ the spectrum shows four resonance lines due to two quadrupole interactions. These spectra indicate that Fe occupies only one crystallographic site in the nonmodulated structure $BiPbSr_2FeO_y$, and two inequivalent sites in the modulated structure $Bi_2Sr_2Cu_{0.6}Fe_{0.4}O_y$. This is consistent with the struc-
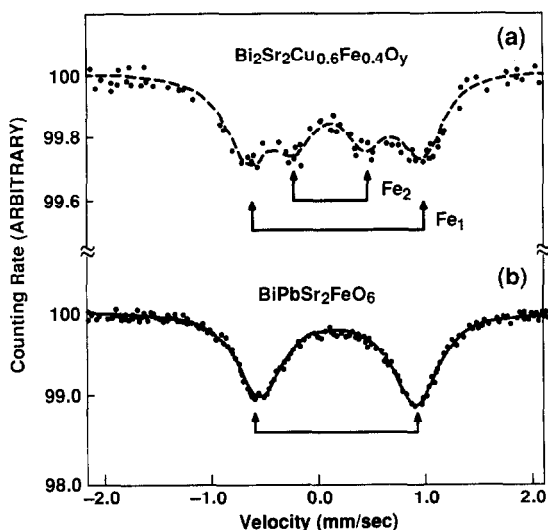
Fig. 5. The room temperature Mössbauer absorption spectra of BiPbSr$_2$MnO$_6$ (a) and of Bi$_2$Sr$_2$Cu$_{0.6}$Fe$_{0.4}$O$_y$ (b). Note the clear evidence for two quadrupole splitting in the undoped Pb sample (b) in contrast to only one quadrupole splitting for the Pb doped sample (a).

Table IV
Room temperature hyperfine parameters (in mm/s) of Bi$_2$Sr$_2$Fe$_{0.4}$Cu$_{0.6}$O$_y$ and BiPbSr$_2$MnO$_6$ compounds.

Compounds	QS(1)	QS(2)	IS(1) [a]	IS(2) [a]
Bi$_2$Sr$_2$Fe$_{0.5}$Cu$_{0.5}$O$_y$	1.64	0.65	0.22	0.18
BiPbSr$_2$FeO$_6$	1.48		0.28	

[a] Isomer shift with respect to Fe metal at room temperature.

ture of BiPbSr$_2$MnO$_y$ and Bi$_2$Sr$_2$MnO$_y$.

The lines are broad for both compounds (full width at half maximum equal to 0.50 mm/s). For the modulated structure, this broadening can be explained both by a random distribution between Fe and Cu in the same crystallographic sites and also by the modulation, but for the unmodulated structure the origin is unknown. The hyperfine parameters determined by nonlinear least-squares fitting to the Mössbauer data are given in table IV. The isomer shifts indicate clearly that Fe is 3+, confirming the TGA results.

3.1. Ambient stability of the BiPb(A)$_2$MO$_y$ phases

To determine the range of stability of these phases in oxygen ambient, TGA measurements were performed. These measurements of weight change were done by heating 20–30 mg specimens to 900°C at 10°C/min in oxygen. The TGA traces are shown in fig. 6. The mass of samples containing Pb increases in two steps, at 500°C and 620°C. In contrast, the samples without Pb have only one step, at higher temperatures. The X-ray powder pattern of the product, after it has been heated above the second step and cooled, shows several phases. Cubic PbO$_{1.44}$ or Bi$_6$Sr(Ca)$_7$O$_{16}$ are the major phases for samples with or without Pb, respectively, and Sr(Ca)MnO$_3$ and Sr(Ca)PbO$_3$ (in which Pb has the oxidation state 4+) were also identified. Thus, all of the samples (except Co containing ones), whether or not they contain Pb, decompose at $T > 780$°C, indicating that these phases are unstable in oxygen, justifying our synthesis work under N$_2$. Finally, when M=Co, as we reported previously, the Bi$_2$Sr$_2$CuO$_y$ phase is stable in oxygen up to 800°C. The addition of Pb reduces its stability range; under oxygen the Pb phase decomposes mainly into the $n = 2$ Co phase plus PbO$_{1.44}$.

To explore the first decomposition step at $T = 500$°C in fig. 6, samples of BiPbSr$_2$MnO$_y$ were
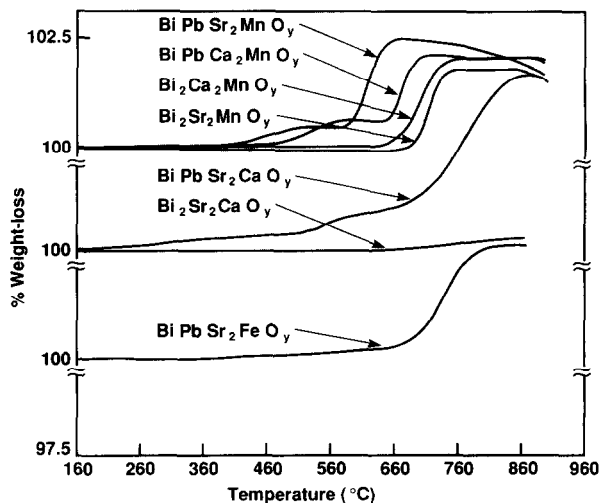
Fig. 6. The TGA traces (weight change) of BiPbA$_2$MO$_6$ (A=Sr, Ca; M=Mn, Co, Fe) heated at 10°C/min to 900°C in oxygen.

heated to 530°C in the TGA, and maintained at this temperature for different times: one second, 2 h and 10 h (samples 1, 2 and 3, respectively). The samples were then rapidly cooled to room temperature and characterized by X-ray diffraction. The X-ray powder pattern for sample 1 is single phase and is similar to that of the initial material, but some of the 2Θ positions of the Bragg peaks shift, and the [2,0,0] and [0,2,0] Bragg peaks merge to within our instrumental resolution. (These peaks also merge in the modulated structures Bi$_2$Sr$_2$MO$_y$).

A least square fit to all the Bragg peaks gives $a = 5.429$ Å, $b = 5.432$ Å and $c = 22.80$ Å for the new unit cell, compared to $a = 5.331$ Å, $b = 5.399$ Å, and $c = 23.757$ Å for the starting material. The c-axis has decreased by about 1 Å. There are two possible explanations for this decrease: the oxidation state of some of the Pb has increased from $2+$ to $4+$, which would decrease the ionic radius of Pb from 1.33 Å to 0.84 Å and so explain the decrease in c; or the oxidation state of Mn has increased from 3 to 4. Since Mn^{3+} is a Jahn–Teller ion and Mn^{4+} is not, the change in oxidation state of Mn would remove the Jahn–Teller distortion, and this would also explain the decrease in c. Magnetic measurements on the oxidized material should allow us to determine the oxidation state of Mn and determine which of these possibilities is correct.

The new phase made at 530°C is metastable. As the annealing time increases, it decomposes into PbO$_{1.44}$ and SrPbO$_3$. The intensity of the Bragg peaks of these decomposition products increases from sample 2 to sample 3. Note that in both these products some of the Pb has oxidation state $4+$.

The uptake in oxygen at 500°C increases the weight by about 0.45% (corresponding to 0.2 oxygen per formula unit). To check the reversibility of this weight change, sample 1 was reannealed under N$_2$ up to 650°C at 10°C/min (fig. 7 curve b), and the resulting material was X-rayed. The weight gain on heating in O$_2$ corresponds within 5% to the weight loss on heating in N$_2$, indicating that the changes in oxygen content are reversible. Moreover, the X-ray powder diffraction patterns of the compound before its treatment in O$_2$ (I) and after its treatment under N$_2$ (III) are identical.

One way to accommodate this extra oxygen is in a structural modulation associated with the periodic

insertion of an extra row of oxygen atom within the BiO layers, as in Bi$_2$Sr$_2$MnO$_y$. To check this, HREM studies were performed on the sample after steps I, II and III. The electron diffraction patterns taken along the 001 are shown in fig. 7, together with the X-ray powder diffraction pattern for the same samples. The electron diffraction patterns I and III are identical, indicating again the reversibility of oxygen uptake. But diffraction pattern II shows extra reflections not observed in I and III; these rows of reflections along a correspond to a modulation of multiplicity 4, just as in Bi$_2$Sr$_2$MnO$_y$ (fig. 4(a)). If the modulation has the same origin as in Bi$_2$Sr$_2$MnO$_y$, this multiplicity corresponds to an increase in oxygen content of 0.25, close to the value of 0.2 inferred from the weight change. Thus the extra oxygen produces a modulation of the structure, and both the oxygen uptake and the modulation disappear reversibly when the oxygen is removed. This is the first example of a direct experimental correlation between reversible oxygen uptake and the structural modulation.

4. Physical properties

Figure 8 displays the variation of the resistance in the a–b plane as a function of the temperature for the single crystals of the Co and Mn (BiPbSr$_2$MO$_y$) phases. The measurements were done using the standard four probe configuration, with a DC current of 5 μA. For all M, the room temperature resistivity is large and increases with decreasing temperature, indicating semiconducting or insulating behavior. Over the temperature range plotted in the figure, the data can be fitted to an Arrhenius law (see insert fig. 8), yielding an activation energy of 0.32 eV and 0.42 eV for the Co and Mn compounds, respectively.

Bi$_2$Sr$_2$MnO$_y$ with M = Mn and Co shows sharp peaks in magnetic susceptibility as a function of temperature [12,14]. The sharpness of the peak has been related to the presence of different Mn sites in the modulated structure [14]. Our preliminary measurements suggest that the phases with Pb also have transitions, but with less pronounced peaks in susceptibility, consistent with the absence of the modulation. Figure 9 compares the susceptibility of single crystals of Bi$_2$Sr$_2$MnO$_{6+y}$ and BiPbSr$_2$MnO$_6$, with
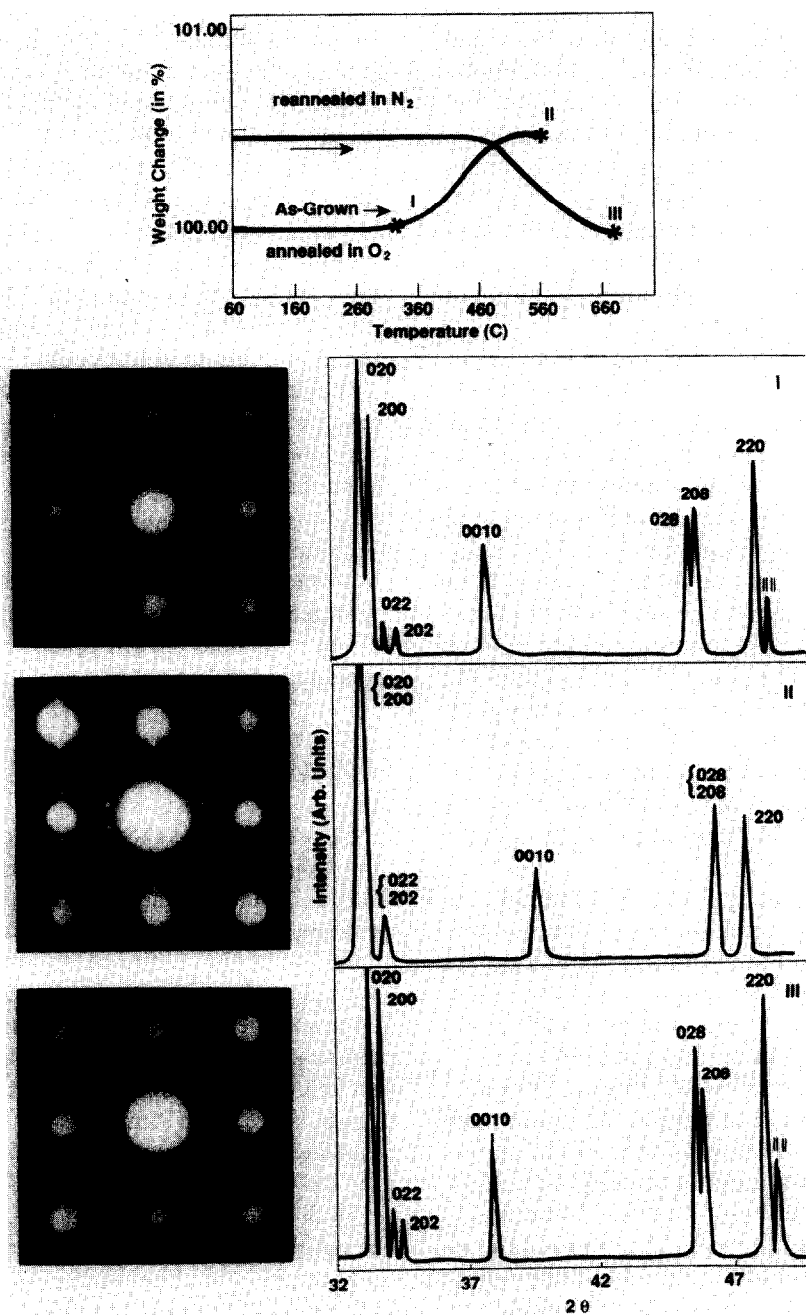
Fig. 7. Thermal analysis of the BiPbSr₂MnO₆ compound. One curve shows the weight gained when the sample is heated in oxygen and the other shows the weight lost when the same sample is reheated in nitrogen. The stars labelled I, II and III indicate the temperature from which the samples were rapidly cooled before X-ray and electron diffraction patterns were taken. The X-ray powder patterns labelled I, II and III are shown over a narrow of 2 T (Cu radiation). On the left of each X-ray powder pattern is its corresponding electron diffraction pattern. Note the reversibility in the changes in oxygen content and structure.
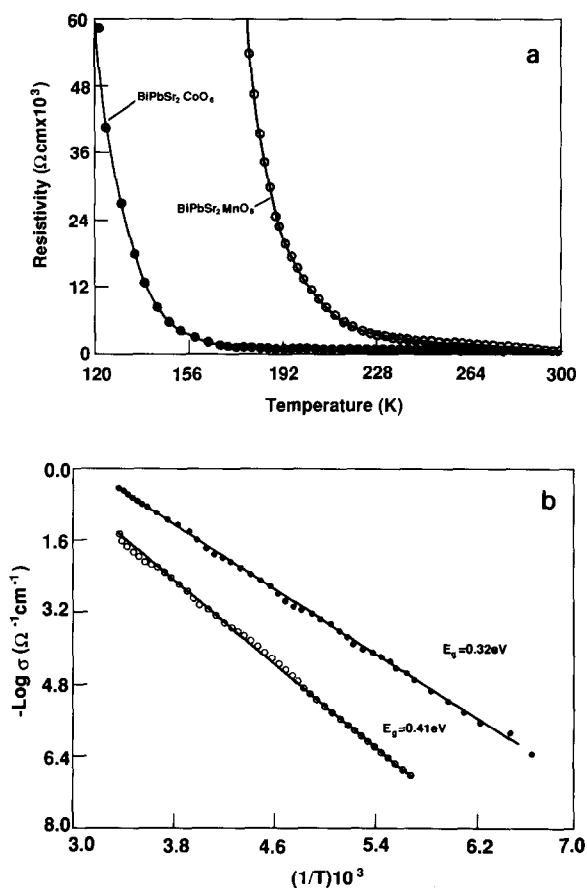
Fig. 8. (a) The temperature dependence of the resistivity in the *ab* plane for BiPbSr₂CoO₆ and BiPbSr₂MnO₆ single crystals. (b) is an Arrhenius plot of the same data.

Fig. 9. The DC magnetic susceptibility (magnetization divided by field) vs. temperature for samples of several crystals of Bi₂Sr₂MnO₆₊ᵧ (total mass 2.4 mg, field 500 G) and BiPb-Sr₂MnO₆ (2.6 mg, 500 G). The data are for increasing temperature, and were measured after the samples were cooled to 6 K in zero field. The field is along the *c*-direction. The insert is an enlargement of the temperature range near the peak for BiPbSr₂MnO₆.

the field along the *c*-direction, measured with a SQUID magnetometer. With addition of Pb, the transition temperature has increased from 120 K to 150 K, but the peak has become much less pronounced (see the insert to the figure). The size of the peak also depends on sample preparation; the peaks in powders, which are prepared at lower temperatures than the single crystals, are stronger and are near 190 K.

Below 40 K, both materials in fig. 9 show history dependence. The data in the figure were measured as the sample warmed, after it had been cooled in zero field. If the samples are cooled in a field, the susceptibility does not decrease below 40 K, but instead remains roughly constant. We are currently studying
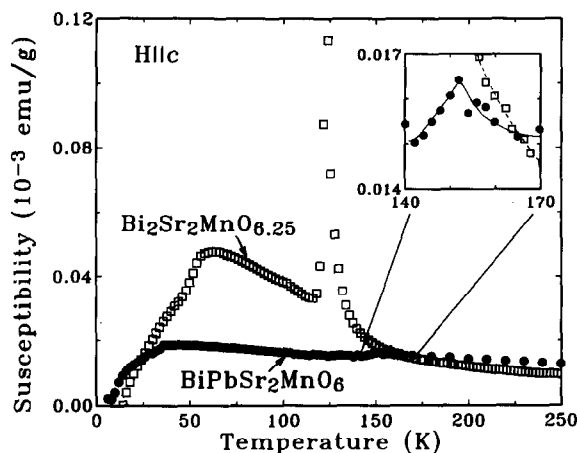
the magnetism in detail in this and the other compounds.

5. Discussion

The similar stereochemistry of Bi(III) and Pb(II) has allowed us to substitute Pb for Bi in the Bi₂Sr₂MOᵧ phase and to synthesize new phases of formula BiPbSr₂MO₆ isostructural to the 10 K superconducting phase, but without modulation. From our single crystal studies of these non-modulated structures, we can now compare the bond lengths in these compounds with previous results for the modulated structure, in order to try to understand how the structural distortion arises and how it affects electronic or magnetic properties.

It has been postulated, based on the observation that the modulation seen in the Bi based cuprates is not found in the Tl-based cuprates, that the modulation could be related to the stereoactivity of the 6s² pairs of Bi(III). These pairs tend to take the place of an anion, distorting the rocksalt layer. If so, one would expect the distortion to be also present in compounds where some Bi has been replaced by Pb,

since Pb(II) ions are isoelectronic with Bi(III) ions and so also have $6s^2$ lone pairs. Thus, the disappearance of the modulation upon Pb substitution shows that the $6s^2$ lone pairs are not the origin of the modulation. (They probably, however, influence the information of the (Bi, Pb)O chains.)

We suggest two contributing factors for the disappearance of the structural modulation when Pb replaces Bi: lattice mismatch, and the oxidation state of the transition metal. Both are probably important, and we consider each in turn.

When Pb replaces Bi, the cell edges *a* and *b* decrease, even though the ionic radius of six-fold coordinated Pb(II), 1.33 Å, is larger than that of six-fold coordinated Bi(III), 1.17 Å. This decrease in *a* can be explained by the increased valence of the transition metal, and suggests that the *a* and *b* parameters are determined by the perovskite slab, not by the (Bi, Pb)O layer. This in turn suggests that the BiO layer is more flexible than the perovskite slab, and can adjust its *a* parameter to match that of the perovskite. This flexibility is consistent with the details of the modulation in $Bi_2Sr_2MnO_{6+y}$ and $Bi_2Sr_3Fe_2O_{9.2}$; the perovskite slabs bend, but with little change in the local environment of each ion, whereas the local coordination of Bi by O varies from a rocksalt to a perovskite environment in the BiO layers.

The problem of matching the (Bi, Pb)O layer onto the perovskite slab is similar to the problems of epitaxial growth, only now we must consider growing a flexibile (Bi, Pb)O rocksalt layer on a less flexible perovskite slab. For a perfect lattice match, the BiO layer should have the rocksalt structure, with the same *a* parameter as the perovskite substrate. The *a* parameter of the BiO layer in the rocksalt structure can be estimated from the bond-valence parameters of Brown and Altermatt [21]. Each Bi is bonded to an O from the adjacent SrO layer, and this bond accounts for 1 of the 3 valence units of Bi^{3+}. The other two units must come from the O in the BiO layer. In a rocksalt layer, each Bi has 4 O at equal distances, so each O has to account for half a valence unit. According to the bond-valence parameters [21], the Bi–O distance would be 2.35 Å, corresponding to an *a* parameter of 4.70 Å. For a PbO rocksalt layer, assuming that the valence of each Pb–O bond is 2/3 of that for the corresponding Bi–O bond, the *a* pa-

rameter would be $a = 5.04$ Å. Since the observed *a* parameters lie in the range of 5.3–5.5 Å, the mismatch for a BiO layer is twice as large as for a PbO layer.

The mismatch between (Bi, Pb)O can be taken up by moving oxygen to form chains. This is an example of the flexibility of these layers. But the larger mismatch for BiO layers with no Pb may rule out this solution to matching the layers, and the modulation may arise as a more drastic mechanism to accommodate the mismatch. In the modulated structure, some regions of the BiO layers are compressed, and the Bi and O atoms locally take up the rocksalt arrangement, while other regions are expanded, with the O between Bi atoms in so-called bridging or perovskite sites. (Placing all the O in bridging sites would give too large an *a* parameter; from the bond-valence parameters, *a* would be 5.94 Å and 6.36 Å for BiO and PbO layers, respectively). As a byproduct of the modulation, extra oxygen is inserted into the BiO layers; this extra oxygen also helps reducing the mismatch by both increasing the lattice parameter of the BiO layers (since the layers now contain more atoms) and by decreasing the *a* parameter of the perovskite slabs (since the extra oxygen increases the valence of the transition metal).

In this first explanation, based on lattice mismatch, the extra oxygen in the BiO layers, while having some benefits, arises almost as an afterthought. On the other hand, this oxygen might be playing a more central role; it could actually be responsible for the modulation, not just a byproduct of it. This oxygen provides a mechanism to increase the valence of the transition metal. If the energy gained in increasing the valence is large enough, the structure will sacrifice elastic energy by distorting, leading to the observed modulation. Thus, from this point of view, the distortion is a mechanism of increasing the valence of the transition metal, not for accommodating a lattice mismatch. Adding Pb is a competing way to increase the valence, because each Pb^{2+} that replaces a Bi^{3+} would allow the valence of a transition metal ion to increase by one, if the oxygen content did not change. Thus, as Pb is added, the driving force for extra oxygen decreases, so the oxygen content decreases with increasing Pb content until eventually the distortion disappears. In short, in this view, the

distortion disappears because the extra oxygen that accompanies it is no longer needed.

Similar reasoning can explain the appearance of the modulation when $BiPbSr_2MnO_6$ is annealed under oxygen. Treatment under oxygen usually favors the metal elements in their high oxidation state, and could increase the oxidation of Pb^{2+} to Pb^{4+} or of Mn^{3+} to Mn^{4+}. The extra oxygen accompanying this valence increase, if inserted in the BiO layers, would then produce the modulation.

Thus we have two explanations for why the modulation occurs, and why it disappears when Pb is added: one based on elastic energy of the lattice mismatch, the other on chemical energy of the transition metal's valence. In fact, the truth probably lies between the two extremes. The modulation provides a way both to accommodate the lattice mismatch and to increase the valence of the transition metal. Adding Pb both decreases the mismatch and provides another way to increase the valence, making the modulation unnecessary for both reasons. As is often the case in arguments like this, it is impossible to say whether the extra oxygen produces the modulation or whether the modulation, as a byproduct, allows extra oxygen to be inserted. We point out, however, that the average of $a/4$ and b for $Bi_2Ca_2MnO_{6+y}$, 5.351 Å, is only 0.03% less than the average of a and b for $BiPbSr_2MnO_{6+y}$, 5.353 Å, and yet the first compound has a modulation and the second one does not. This suggests that the mismatch alone is not enough, and that the chemical driving force for introducing extra oxygen into the BiO layers must also be important.

In the new $Bi_{2-x}Pb_xSr_2MO_y$ compounds, the Pb content x can be as large as 1. In contrast, in the Bi-based cuprates, x is limited to 0.3 or 0.5. The most obvious reason for this limit in the cuprates is the difficulty in forming Cu^{3+}. An oxidation state of $+III$ is common for all the 3d metals except Cu. The redox chemistry of Cu is different from that of the other 3d metals and most of the known oxide compounds containing $Cu(III)$ can only be made using high pressures of oxygen. Thus, it is probably the difficulty in stabilizing $Cu(III)$ that limits the solubility range of Pb in the Bi cuprates.

In fact, it appears that a Cu valence of about 2.4 is close to the limit of what can be achieved in these compounds, although this limit seems to decrease as

more Cu layers are added to the unit cell. In the 2201 phase ($Bi_{2-x}Pb_xSr_2CuO_{6+y}$), a Cu valence of 2.4 is produced by $x=0.4$, close to the limit of $x=0.5$ observed [27]. At this composition, the resistivity still shows a superconducting transition, confirming that the valence of Cu is above 2. Moreover, the difference between a and b increases with Pb content, just as we find here for compounds with other transition metals. In the 2212 and 2223 Cu phases ($Bi_{2-x}Pb_xSr_2CaCu_2O_{8+y}$ and $Bi_{2-x}Pb_xSr_3Ca_2Cu_3O_{10+y}$), the limits of Pb solubility are $x=0.6$ [18] and $x=0.4$ [17]. Again, these limits correspond to the values expected if the Cu valence remains constant as Pb is added, and at the same time the oxygen associated with the modulation is removed. (The multiplicity of the modulation is about 5 sublattice periods.) But the limiting Cu valence is smaller than in 2201: 2.3 for 2212, and 2.13 for 2223.

In $Bi_2Sr_2YCu_2O_y$, the oxygen content is about 8.6 (although the extra oxygen has not been located in the structure by diffraction). Again, as Pb is added, the oxygen content decreases; adding one Pb per formula unit decreases the oxygen content by 0.5, again implying that the Cu valence stays roughly constant.

Thus, in the bismuth cuprates the maximum Pb content x appears to be determined by a limit to the Cu valence. Moreover, adding any Pb changes the O content, to keep the Cu valence constant. The solubility of Pb is limited to about 0.4 in this way. For the other transition metals M, however, the valence of M increases from 2.5 to $3+$ as Pb is added, and the limit to the solubility of Pb is about 1.

Although the valence of M eventually reaches 3, there are two ways it might vary with Pb content x when x is small. The valence could initially remain constant, in which case the oxygen content would have to vary with x until the modulation disappeared. Alternatively, the valence could increase immediately, allowing the oxygen content to remain constant until the valence of M reaches 3. In the first case, the period of the modulation would vary with x at small x, but in the second it would not. The small change in the modulation between $x=0$ and $x=0.25$ in $BiPbSr_2MnO_6$, from 4 to less than 4.2, suggests that it is the second case that applies.

This work has not resolved why the modulation in compounds like $Bi_2Sr_2MO_{6+y}$ usually has a wave-

length of 4 times the subcell repeat distance. The valence of the 3d metal is not the limit, because the valence can increase from 2.5 to 3 as Pb is added. Perhaps the slabs are bent as much as they can be at this wavelength, so that the multiplicity 4 is the elastic limit of the modulation. In Bi$_2$Sr$_3$Fe$_2$O$_{9.2}$, the slabs are thicker and consequently more rigid, which might be why the multiplicity is 5 in this compound.

In summary, we have reported the synthesis of phases of general formula BiPbA$_2$MO$_6$ (A = Ca, Sr; M = Co, Fe, Mn) whose structure is closely related to that of the Bi$_2$Sr$_2$MO$_y$ phase, but without the structural modulation. We proposed what when trivalent Bi is replaced by divalent Pb, the extra oxygen in the BiO layers that produces the structural distortion is no longer needed to maintain charge neutrality, and so the structural distortion disappears. We confirmed that the structural distortion involves extra oxygen by showing for the first time that the modulation can appear or disappear reversibly when the oxygen content changes. Although these new phases are not superconducting, they are derived from phases (those without Pb) that exhibit unusual magnetic properties. We are currently studying the dependence of these properties on the structural modulation, hoping that such information may also help us understand the interplay between magnetism and superconductivity in the high-T_c cuprates.

Acknowledgements

References

[1] G. Bednorz and K.A. Muller, Z. Phys. B64 (1986) 189.
[2] M.K. Wu, J.R. Ashburn, C.J. Torng, P.H. Hor, R.L. Meng, L. Gao, Z.J. Huang, Y.Q. Wang and C.W. Chu, Phys. Rev. Lett. 58 (1987) 908.
[3] J.E. Greedan, A. O'Reily and C.V. Stager, Phys. Rev. B35 (1987) 8770.
[4] Y. LePage, W.R. McKinnon, J.M. Tarascon, L.H. Greene, G.W. Hull and D.M. Hwang, Phys. Rev. B35 (1987) 7249.
[5] J.M. Tarascon, Y. LePage, P. Barboux, B.G. Bagley, L.H. Greene, W.R. McKinnon, G.W. Hull, M. Giroud and D.M. Hwang, Phys. Rev. B37 (1988) 9382.
[6] S.A. Sunshine et al., Phys. Rev. B38 (1988) 893.
[7] M.A. Subramanian, C.C. Torardi, J.C. Calabrese, J. Gopallakrishnan, K.J. Morissey, T.R. Askew, R.B. Flippen, U. Choudry and A.W. Sleight, Science 239 (1988) 1015.
[8] H. Maeda, Y. Tanaka, M. Fuksutmi and T. Asano, Jpn. J. Appl. Phys. 27 (1988) L209.
[9] Z.Z. Sheng and A.M. Hermann, Nature 332 (1988) 138.
[10] G. Xiao, F.H. Streiz, A. Gavrin, Y.W. Du and C.L. Chien, Phys. Rev. B35 (1987) 8782.
[11] J.M. Tarascon, P. Barboux, P.F. Miceli, L.H. Greene and G.W. Hull, Phys. Rev. B37 (1988) 7458.
[12] J.M. Tarascon, P.F. Miceli, P. Barboux, D.M. Hwang, G.W. Hull, M. Giroud, L.H. Greene, Y. LePage, W.R. McKinnon, E. Tselepis, G. Pleizier, M. Eibschutz, D.A. Neuman and J.J. Rhyne, Phys. Rev. B39 (1989) 11587.
[13] J.M. Tarascon, R. Ramesh, P. Barboux, M.S. Hedge, G.W. Hull, L.H. Greene and M. Giroud, Solid State Commun. 71 (1989) 663.
[14] W.R. McKinnon, E. Tselepis, Y. LePage, S.P. McAlister, G. Pleizier, J.M. Tarascon, P.F. Miceli, R. Ramesh, G.W. Hull, J.V. Waszczak, J.J. Rhyne and D.A. Neumann, Phys. Rev. B, in press.
[15] Y. LePage, W.R. McKinnon, J.M. Tarascon and P. Barboux, Phys. Rev. B40 (1989).
[16] J.M. Tarascon, Y. LePage, W.R. McKinnon, E. Tselepis, P. Barboux, B.G. Bagley and R. Ramesh, Proc. MRS Meeting, 1989.
[17] U. Endo, S. Koyama and T. Kawai, Jpn. J. Appl. Phys. 27 (1988) L1476.
[18] N. Fukushima, H. Niu, S. Nakamura, S. Takeno, M. Hayashi and K. Ando, Physica C 159 (1989) 777.
[19] Y. LePage, P.S. White and E.J. Gabe, Proc. Am. Crystallogr. Association Meeting, Program Abstracts Series 2, vol. 14 (ACA, New York, 1986) Abstract PA 23, 24.
[20] E.J. Gabe, A.C. Larson, F.L. Lee and Y. LePage, Crystallographic Computing 3: Data Collection, Structure Determination, Proteines and Databases, eds. G.M. Sheldrick et al. (Oxford Univ. Press, New York, 1985) 167.
[21] I.D. Brown and D. Altermatt, Acta Cryst B41 (1985) 244.
[22] C.C. Torardi, M.A. Subramanian, J.C. Calabrese, J. Gopalakrishnan, E.M. McCarron, K.J. Morrissey, T.R. Askew, R.B. Flippen, U. Chowdry and A.W. Sleight, Phys. Rev. B38 (1988) 225.
[23] A.F. van der Elzen and G.D. Rieck, Acta Cryst B29 (1973) 2936.
[24] B. Raveau, C. Michel, M. Hervieu, D. Groult and J. Provost, Proc. 1989 Spring MRS meeting, High Temperature Superconductors: Relationships Between Properties, Structure and Solid State Chemistry, vol. 156 (1989) 129.
[25] C.C. Torardi et al., private communication.
[26] J.M. Tarascon, Y. LePage and W.R. McKinnon, Eur. J. Inorganic Chem. (First issue), in press.
[27] A. Maeda, Y. Kato, T. Shibauchi, Y. Nakajima, H. Watanabe and K. Uchinokura, Jpn. J. Appl. Phys. 28 (1989) L2549.